

Coexistence of antiferrodistortive and ferroelectric distortions at the PbTiO_3 (001) surface

Claudia Bungaro* and K. M. Rabe

Department of Physics and Astronomy, Rutgers University, Piscataway, NJ 08854-8019, USA.

(Dated: November 5, 2018)

The $c(2 \times 2)$ reconstruction of (001) PbTiO_3 surfaces is studied by means of first principles calculations for paraelectric (non-polar) and ferroelectric ([001] polarized) films. Analysis of the atomic displacements in the near-surface region shows how the surface modifies the antiferrodistortive (AFD) instability and its interaction with ferroelectric (FE) distortions. The effect of the surface is found to be termination dependent. The AFD instability is suppressed at the TiO_2 termination while it is strongly enhanced, relative to the bulk, at the PbO termination resulting in a $c(2 \times 2)$ surface reconstruction which is in excellent agreement with experiments. We find that, in contrast to bulk PbTiO_3 , in-plane ferroelectricity at the PbO termination does not suppress the AFD instability. The AFD and the in-plane FE distortions are instead concurrently enhanced at the PbO termination. This leads to a novel surface phase with coexisting FE and AFD distortions which is not found in PbTiO_3 bulk.

PACS numbers:

I. INTRODUCTION

The ABO_3 perovskite structure exhibits several lattice instabilities which lead to a rich variety of phase diagrams with structures ranging from non-polar antiferrodistortive (AFD) to ferroelectric (FE) and antiferroelectric (AFE). In these systems, polar and non-polar instabilities often compete and tend to suppress one another. For instance, in SrTiO_3 it has been found that ferroelectricity is enhanced if the AFD degrees of freedom are artificially frozen out by setting the corresponding distortion to zero.^{1,2} Of these various instabilities, the polar instabilities are the ones responsible for the technologically important and fundamentally interesting properties, such as ferroelectricity and large piezoelectric and dielectric responses.

Currently there is a great deal of effort being expended to develop nanoscale devices. If nanoscale systems based on ferroelectricity are to be feasible, then the polar instabilities must remain dominant down to the nanoscale. In systems of reduced dimensionality, such as thin films or nanoparticles, a substantial fraction of the material is found in proximity to a surface, and surface effects may become important. The surface can affect the material behavior by modifying the strength of the various instabilities and their interactions leading to novel phases not present in bulk systems.

Lead titanate (PbTiO_3) is the prototype of a large class of Pb-based perovskites. The cubic perovskite structure of PbTiO_3 possesses several branches of unstable phonons, including FE instabilities which consist of zone-center polar TO modes and AFD instabilities which consist of nonpolar zone-boundary modes involving rotations of oxygen octahedral cages surrounding the Ti atoms.³ In bulk PbTiO_3 , the FE and AFD instabilities of the cubic structure compete with each other and the FE lattice distortion suppresses the AFD distortion so that AFD distortions do not participate in the ground-state tetrag-

onal FE structure. The possible impact of the proximity of the surface on lattice instabilities and their mutual interactions is thus of great importance in understanding the structure and properties of PbTiO_3 surfaces and ultrathin films.

Previous theoretical studies on lead titanate have been confined to the behavior of the polar FE instability at the (001) surface.^{4,5,6} These studies employed (1×1) surface periodicity, which by construction does not permit AFD deformations. Proximity to the surface, however, could enhance the strength of non-polar instabilities and modify their interaction with the FE instability. Indeed, an AFD $c(2 \times 2)$ reconstruction has recently been found at the (001) surface of PbTiO_3 using grazing incidence x-ray scattering,⁷ suggesting that the AFD instability is important at the surface.

In the following, we study the behavior of the AFD instability and its possible competition with ferroelectricity at the PbTiO_3 (001) surface using first-principles calculations. Initially we study the AFD distortion at the surface, using symmetry constraints to freeze out polar distortions; next we relax this constraint and study the competition between the AFD and in-plane FE distortions at the PbO -terminated surface, which is the equilibrium termination for PbTiO_3 (001)⁵.

In the absence of ferroelectricity, we find that the impact of the surface is termination-dependent: at the PbO -terminated surface, the strength of the AFD instability is enhanced relative to the bulk; while at the TiO_2 terminated surface, the strength of the instability is diminished. At the PbO -surface, in contrast to the bulk, where the presence of ferroelectricity suppresses AFD, we find that the two coexist and we observe a $c(2 \times 2)$ reconstruction that agrees very well with experiment.⁷

The paper is organized as follows: section II is devoted to the theoretical method and the technical details of our calculations. In section III we study the AFD instability in bulk cubic lead titanate. In section IV we study the

surface effect upon the AFD distortion in absence of FE distortion. The competition of AFD and in-plane FE distortions in the near-surface region is studied in section V. The conclusions are summarized in section VI.

II. THEORETICAL METHOD

Our theoretical study is based on ab initio calculations that were performed within density-functional theory (DFT) using the plane-wave pseudopotential method as implemented in the PWSCF package⁸. In this section we describe the technical details of the calculations and the supercells used to study the surface of PbTiO_3 (001) films.

A. Computational details

The exchange and correlation energy was given within the local density approximation (LDA) using the parameterization of Perdew and Zunger⁹. Ultrasoft pseudopotentials¹⁰ were used to describe the electron-ion interaction, treating as valence states the $3s$, $3p$, $3d$, and $4s$ states of Ti, the $4s$, $4p$, $4d$, and $5s$ states of Zr, the $5d$, $6s$, and $6p$ states of Pb, and the $2s$ and $2p$ states of O. The wave-functions were expanded in plane waves with an energy cutoff of 25 Ry. A larger cutoff of 250 Ry was used for the charge density, which includes the augmentation charges required by the use of ultrasoft pseudopotentials. The Brillouin zone (BZ) integration was performed using a (3,3,2) Monkhorst-Pack mesh¹¹ in the Brillouin zone of the $c(2\times 2)$ supercells. Relaxations of atomic coordinates have been iterated until the forces on the atoms were less than 0.001 Ry/a.u. (26 meV \AA^{-1}).

B. Surface and slab geometries

In PbTiO_3 , the stacking along [001] consists of alternating TiO_2 and PbO atomic layers (see Fig. 1). There are two possible terminations for the non-polar (001) surface: the PbO -terminated surface and the TiO_2 -terminated surface. We have studied both types of surface termination.

The surfaces were modeled using a periodic slab geometry. Specifically, we used symmetric slabs, terminated by two equivalent surfaces, and separated by a vacuum region of approximately 14 \AA . For the PbO -termination we used slabs of 11 atomic layers (7-layer slabs were used for direct comparison with previous calculations), and for the TiO_2 termination we used slabs of 9 atomic layers. A $c(2\times 2)$ in-plane supercell was used, containing 4 atoms in each PbO layer and 6 atoms in each TiO_2 layer (Fig. 1). The in-plane lattice parameter is $a_0\sqrt{2}$, where $a_0=7.37$ a.u. is the theoretical lattice parameter of cubic PbTiO_3 bulk. This mimics the epitaxial constraint imposed by a lattice-matched cubic substrate.

In order to investigate the behavior of the AFD distortion in the absence of FE distortions, we studied non-polar (paraelectric) $c(2\times 2)$ films. Specifically, we relaxed the atomic positions in the lowest symmetry space group containing inversion ($P2/m$),¹² as this allows for the largest number of degrees of freedom for the atomic displacements during the energy minimization while constraining the spontaneous polarization to zero. With this symmetry, all the atoms are allowed to move in the z (surface normal) direction and the oxygen atoms in the TiO_2 layers are also allowed to move in the xy plane (parallel to the surface). All the other atoms are fixed by symmetry to the ideal perovskite coordinates in the xy plane. All the symmetry-allowed displacements were fully relaxed to find the equilibrium structure which minimizes the energy.

The competition between the AFD and FE distortions was studied using a ferroelectric film with in-plane polarization. This is achieved by using a symmetric $c(2\times 2)$ slab with space group Pm .¹³ The mirror symmetry, M_z , prevents spontaneous polarization in the z direction and allows only an in-plane polarization to develop in the film.

The case of perpendicular polarization is not considered in this work because it requires special treatment of the electrical boundary conditions and a separate discussion.¹⁴

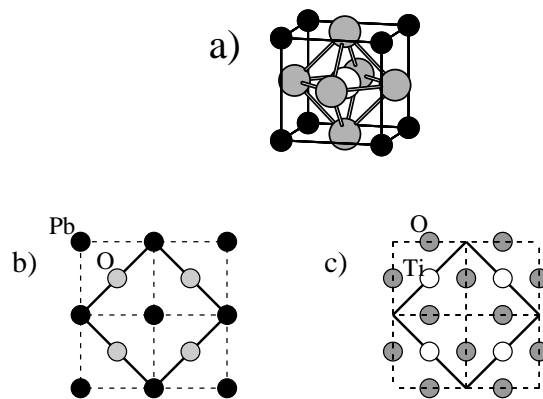


FIG. 1: (a) Crystal structure of the ideal cubic perovskite unit cell of PbTiO_3 . In (b) and (c) are top views of the ideal PbO and TiO_2 (001) atomic layers; the solid lines indicate the $c(2\times 2)$ surface unit cells.

The atomic structure was optimized by relaxing the symmetry-allowed atomic displacements. We defined atomic displacements, δ_α , relative to the ideal perovskite structure. Atomic relaxations normal to the surface, δ_z , cause a rumpling of the atomic layers and a change in interlayer distances relative to the ideal cubic structure. The in-plane atomic relaxations, δ_\parallel , chiefly consist of rotations of the oxygen squares surrounding the Ti atoms in the TiO_2 planes.

To analyze the optimized structures and compare with

previous results we computed the following parameters: the rumpling amplitude, η_i , in each layer, i , the change in the interlayer distances relative to the ideal cubic structure, Δd_{ij} , and the rotation angle of the oxygen squares in the TiO_2 planes, θ_i .

The structural parameters are defined as follows. For each atomic plane, i , we let $\bar{\delta}_z(\text{O}_i)$ and $\bar{\delta}_z(\text{M}_i)$ be the average z displacements of the oxygen and metal atoms, respectively. As in Ref. 5, the interlayer distance d_{ij} is given by the difference of the averaged $\bar{\delta}_z$ displacements, $[\bar{\delta}_z(\text{O}_i) + \bar{\delta}_z(\text{M}_i)]/2$, computed for layer i and j . The layer rumpling is given by $\eta_i = [\bar{\delta}_z(\text{M}_i) - \bar{\delta}_z(\text{O}_i)]$. A negative rumpling, $\eta_i < 0$, means that on average the metal atoms are deeper inside the surface relative to the O atoms. The rotation angles θ_i are zero for the (1×1) surface, a value different from zero indicating a $c(2 \times 2)$ reconstruction.

III. ANTIFERRODISTORTIVE INSTABILITY IN BULK CUBIC PbTiO_3

To understand how the AFD instability is modified near the surface we first study the AFD distortion in bulk PbTiO_3 . The rotation of oxygen octahedra is a common AFD instability in perovskite oxides. In bulk cubic PbTiO_3 it is associated with two unstable zone-boundary phonons: the R_{25} mode at the R point of the Brillouin zone, $\mathbf{q}=(111)\pi/a$, and the M_3 mode at the M point, $\mathbf{q}=(110)\pi/a$. The three-fold degenerate R_{25} mode can be chosen to correspond to the rotations, about the $\langle 001 \rangle$ Cartesian axes, of TiO_6 octahedra in opposite directions from one cubic unit cell to the next. The singly-degenerate M_3 mode is similar to the R_{25} mode, but neighboring planes of octahedra along the rotation axis rotate in-phase instead of out-of-phase.

We considered distorted structures obtained by separately “freezing in” R_{25} and M_3 modes in cubic PbTiO_3 at the theoretical cubic lattice constant ($a_0=7.37$ a.u.). In Fig. 2 we show the computed values of the total energy per 5-atom unit cell as a function of the rotation angle. The energy is lowered by the AFD distortion, as expected, and the R_{25} distortion with rotation along a Cartesian axis is more favorable than the related M_3 distortion. The computed equilibrium value of the octahedral rotation angle is $\theta_{\text{bulk}} = 3.3^\circ$, and the energy gain associated with the AFD instability in the bulk is $\Delta E_{\text{AFD}}^{\text{bulk}} = 1.2$ meV per bulk unit cell (well depth in Fig. 2).

The small energy gain indicates that cubic PbTiO_3 , in the absence of any FE distortion, displays only a weak AFD instability. In particular, it is much weaker than the ferroelectric instability, which has a well depth of about 15 meV for the cubic undistorted unit cell (and about 50 meV per unit cell if coupling with the tetragonal distortion is included).

The AFD instability is suppressed by the FE distortion. In fact the ground-state ferroelectric tetragonal structure with 5 atoms per unit cell has no unstable

phonons at any wavevector¹⁵. The ferroelectric structure results from the coupling of a FE polar distortion (TO mode) and a tetragonal strain. We checked, therefore, if the suppression of the AFD instability can be caused by the FE distortion alone. To do this we first relaxed the ferroelectric distortion without coupling to tetragonal strain by keeping the unit cell fixed to the ideal cubic structure and allowing internal atomic displacements along the (001) direction. As a result a spontaneous polarization develops along the (001) direction. We then computed the phonons for this “cubic polarized” structure (C-FE) and found no unstable modes at the R point of the Brillouin zone. We conclude that the FE distortion suppresses the AFD instability even in absence of tetragonal strain.

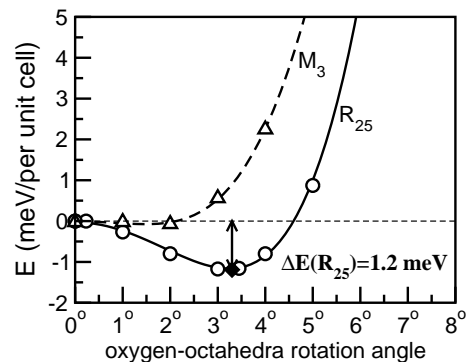


FIG. 2: Energetics of the AFD instability in bulk cubic PbTiO_3 . Filled diamond indicates the minimum, $\theta = 3.3^\circ$ and $\Delta E = 1.2$ meV per bulk unit cell, to be compared with the ferroelectric well depth, $\Delta E = 50$ meV per bulk unit cell. Triangles and circles are calculations for the M_3 and R_{25} distortions, respectively. The solid line is a polynomial interpolation.

IV. PbTiO_3 (001) SURFACES IN THE ABSENCE OF FERROELECTRIC DISTORTIONS

To understand the behavior of non-polar distortions near the surface, we study the atomic structure of the non-polar (paraelectric) films. We studied both the PbO and TiO_2 terminations with $c(2 \times 2)$ in-plane translational symmetry. Our primary focus in this section will be on characterizing the $c(2 \times 2)$ reconstruction and its dependence on termination.

A. PbO termination

Results for the atomic displacement and structural parameters of the optimized $c(2 \times 2)$ surface structure, shown in Fig. 3, are presented and compared with those for the (1×1) surface in Tables I and II.

The results for the (1×1) surface are in excellent agreement with a previous calculation⁵, given in Table II.

Small differences are chiefly due to the different slab thickness used in the two calculations (we obtained almost identical results using a 7-layer slab as in Ref.5). We used a thicker 11-layer slab to study the behavior of lattice distortions in the near-surface region and their decay to bulk-like behavior in the central layers of the slab. The change in interlayer distance displays an oscillating behavior: the first interlayer distance, d_{12} , is substantially contracted, whereas the second, d_{23} , is expanded and the third, d_{34} , is again contracted. The most noticeable features is the large inward displacement of the surface Pb atom relative to the surface O atom. This accounts for the large first interlayer contraction, Δd_{12} , and first layer rumpling, η_1 .

TABLE I: Atomic displacements, relative to the ideal cubic perovskite structure, for the PbO-terminated (001) surface of non-polar PbTiO₃ films. The relaxations perpendicular (δ_z) and parallel (δ_{\parallel}) to the surface are given as a percentage of the cubic lattice parameter a_0 .

layer	atom	c(2×2)		(1×1)
		δ_z	$ \delta_{\parallel} $	δ_z
1	Pb	-1.83	10.03	-4.34
	O	-0.39		-0.41
2	Ti	+2.79		+2.67
	O	+1.85		+1.26
3	Pb	-1.57		-2.08
	O	+0.41		-0.35
4	Ti	+0.51		+0.64
	O	+0.09		+0.15
5	Pb	-0.25		-0.56
	O	-0.02		-0.11
6	Ti	0	0	
	O	0	3.43	0

The optimized atomic structure for the PbO termination of the non-polar c(2×2) PbTiO₃ (001) film is shown in Fig. 3, displaying the large c(2×2) reconstruction occurring in the TiO₂ subsurface layer. The reconstruction consists of alternating clockwise and anti-clockwise rotations of the Ti-centered oxygen squares in the TiO₂ layer. The in-plane oxygen displacements are 10% of the bulk lattice parameter, corresponding to a rotation angle of $\theta_1=11^\circ$. This atomic distortion is essentially an AFD rotation of the surface oxygen-octahedra about the z axis; particularly noteworthy is the substantial enhancement of the AFD distortion at the PbO-terminated surface. Neighboring planes of octahedra along the rotation axis rotate out of phase, as in the dominant AFD bulk instability (R_{25} mode). Deep inside the film, the AFD distortion recovers its bulk value in the absence of a ferroelectric distortion. The relaxation energy, relative to the ideal (1×1) surface, is -0.29 and -0.18 eV per (1×1) surface unit cell for the c(2×2) and (1×1) surfaces, respectively. The c(2×2) reconstructed surface is much more

TABLE II: Structural parameters for the PbO-terminated (001) surface of non-polar PbTiO₃ films. Change in the interlayer distance, Δd_{ij} , and layer rumpling, η_i , in percent of the lattice constant a_{bulk} . Rotation angle, θ_i , of the oxygen squares in the TiO₂ layers. Relaxation energy relative to the ideal (1×1) surface, ΔE_{relax} , in eV per (1×1) surface unit cell.

	this work		Meyer et al. ^a
	c(2×2)	(1×1)	(1×1)
Δd_{12}	-3.4	-4.3	-4.2
Δd_{23}	+2.9	+3.2	+2.6
Δd_{34}	-0.9	-1.6	-0.8
Δd_{45}	+0.4	+0.7	
Δd_{56}	-0.1	-0.3	
η_1	-1.4	-3.9	-3.9
η_2	+0.9	+1.4	+1.2
η_3	-2.0	-1.7	-1.2
η_4	+0.4	+0.5	
η_5	-0.2	-0.4	
θ_2	11.4°	0	0
θ_4	-2.9°	0	0
θ_6	3.9°	0	
(θ_{bulk})	(3.3°)		
ΔE_{relax}	-0.29	-0.18	

^aRef.5

favorable than the relaxed (1×1) surface, the difference in energy being 0.11 eV per (1×1) surface unit cell. It is interesting to notice that the symmetry of the relaxed structure (space group P4/nmm) is higher than the minimal symmetry constraint imposed during energy minimization (space group P2/m). The four oxygen atoms in each TiO₂ layer are equivalent by symmetry in the relaxed structure.

The main differences between the c(2×2) and (1×1) structures are (i) the AFD rotation of the TiO₄-squares, chiefly in the second layer, (ii) a much smaller inward displacement of the surface Pb atoms, $\delta_z(\text{Pb}_1) = -1.83\%$ of a_0 , (iii) and, consequently, a substantial reduction of the first layer rumpling (η_1) and the first interlayer contraction (Δd_{12}).

These results can be understood in terms of the particular chemistry of lead. In the ideal cubic perovskite bulk, Pb is in the center of an O₁₂ cage and the twelve equivalent Pb-O bonds are 2.76 Å long. The tendency of lead to move off-center and form stronger covalent PbO bonds, as short as 2.59 Å, has been demonstrated to be an important factor in ferroelectricity in PbTiO₃.^{16,17} Formation of shorter bonds is favored in the broken symmetry environment at the surface and, as we discuss next, can be regarded as the driving force for the c(2×2) AFD reconstruction occurring at the PbO-terminated surface.

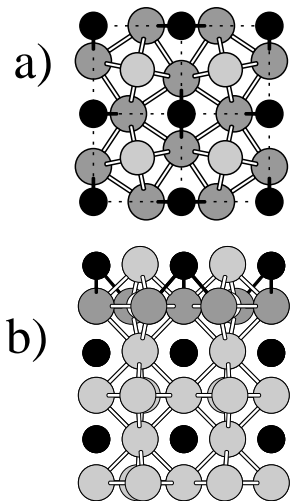


FIG. 3: Optimized atomic structure of the $c(2 \times 2)$ non-polar (001) PbTiO_3 film with PbO surface termination. (a) Top view; only the first top two layers are shown. (b) Side view; only the top half of the 11-layer slab is shown. The oxygen atoms in the second layer are shown in a darker shade of gray. The $c(2 \times 2)$ AFD reconstruction, consisting of rotation of the Ti-centered oxygen squares in the TiO_2 subsurface layer, is clearly visible. Only Pb-O bonds shorter than 2.6 \AA are shown (in black); they are 2.39 \AA long.

In Table III we show the values of the interlayer bondlengths computed for the $c(2 \times 2)$ and (1×1) surfaces. Each Pb atom forms four bonds with the in-plane oxygen atoms, four interlayer bonds with O atoms in the plane above, and four interlayer bonds with O atoms in the plane below; the surface Pb atom is undercoordinated and has eight bonds (four in-plane bonds and four interlayer bonds with the plane below). In the non-polar slab, in-plane Pb off-centering is not allowed by symmetry. Thus, the four equivalent in-plane Pb-O bonds can only change by bending; their lengths are essentially fixed to 2.76 \AA and are not included in Table III. In contrast, the interlayer Pb-O bonds can stretch or contract substantially. When a (1×1) periodicity is enforced, the only possibility to shorten the Pb-O bond, as found in Ref. 5, is by a large downward displacement of the surface Pb atom, resulting in bondlengths (2.61 \AA long) comparable to those in tetragonal FE bulk. At the $c(2 \times 2)$ surface the AFD distortion offers an alternative way, evidently more energetically favorable, to form fewer but shorter Pb-O bonds. Each surface Pb atom has four oxygen neighbors in the subsurface TiO_2 layer. Rotation of the TiO_4 -squares brings two of these much closer, resulting in even stronger bonds (2.39 \AA long) only a bit longer than those in bulk PbO (2.32 \AA long, experimental value¹⁸). The rotation also shortens significantly two of the bondlengths for the Pb_3 atom to 2.60 \AA , comparable to those in tetragonal FE bulk. Since the rotation provides a more effective alternative mechanism for shortening Pb-O bonds, the inward displacement of

surface Pb atoms (and the related rumpling η_1 and interlayer contraction Δd_{12}) is substantially reduced with respect to the (1×1) surface. The average bond length for each Pb atom does not change much between the $c(2 \times 2)$ and (1×1) surfaces and it is not much different from the undistorted bond length.

As a further verification of the particular role of lead in the enhancement of the AFD distortion at the surface, we have relaxed the non-polar (001) surface of BaTiO_3 . The Ba-O bond has a more ionic character and is therefore a good contrasting example. We find no AFD distortion at the BaO surface. This confirms that the formation of stronger covalent bonds is the origin of the AFD reconstruction at the PbO -terminated (001) surface of PbTiO_3 .

Finally we notice that, contrary to the Pb-O bonds, the interlayer Ti-O bonds are almost the same at the $c(2 \times 2)$ and (1×1) surfaces, and their values reflect the alternating contraction and expansion of the interlayer distances.

TABLE III: Computed values for the Pb-O and Ti-O interlayer bond lengths (in \AA) at the PbO terminated $c(2 \times 2)$ and (1×1) surfaces of the non-polar (001) PbTiO_3 film. For comparison, the in-plane Pb-O bond length is 2.76 \AA . Average bond lengths $\text{Pb}_i\text{-O}$ for each Pb_i atom are given in the “average” columns. The labels i and j indicate the atomic planes, with $i, j=1$ being the first surface layer. Shorter Pb-O bonds are highlighted in bold.

	$c(2 \times 2)$ surface			(1×1) surface	
$\text{Pb}_i\text{-O}_j$	short	long	average	average	
$\text{Pb}_1\text{-O}_2$	2.39	2.96	2.72	2.61	2.69
$\text{Pb}_3\text{-O}_2$	2.60	3.13	2.78	2.85	2.77
$\text{Pb}_3\text{-O}_4$	2.64	2.78		2.70	
$\text{Pb}_5\text{-O}_4$	2.70	2.84	2.76	2.78	2.76
$\text{Pb}_5\text{-O}_6$	2.66	2.85		2.74	
<hr/>					
$\text{Ti}_i\text{-O}_j$					
$\text{Ti}_2\text{-O}_1$	1.83			1.83	
$\text{Ti}_2\text{-O}_3$	2.04			2.07	
$\text{Ti}_4\text{-O}_3$	1.95			1.91	
$\text{Ti}_4\text{-O}_5$	1.97			1.98	
$\text{Ti}_6\text{-O}_5$	1.95			1.95	

B. TiO_2 termination

The computed structural parameters for the TiO_2 termination of the non-polar film are summarized in Table IV. As we discuss in detail below, the large AFD surface reconstruction observed at the PbO termination does not occur at the TiO_2 termination.

Our results for the (1×1) TiO_2 surface are in very good agreement with previous calculations. The structure of

the optimized $c(2\times 2)$ supercell is little changed from that obtained for the (1×1) slab. The only difference is a small AFD rotation of the oxygen octahedra in the inner layers, which is due to the AFD instability of bulk PbTiO_3 in absence of FE distortion. The AFD rotation in the first surface layer is essentially zero ($\theta_1 = 0.1^\circ$) indicating that, in contrast to the PbO termination, the AFD instability is weakened at the TiO_2 termination. The optimized $c(2\times 2)$ and (1×1) structures have the same energy within numerical accuracy (they differ by less than 10^{-6} Ry per atom).

Mayer et al.⁵ have shown that in thermodynamic equilibrium, the (1×1) PbO-termination is always more stable than the (1×1) TiO_2 -termination. Our results show that the TiO_2 -termination does not reconstruct while the PbO-termination is further stabilized by the AFD $c(2\times 2)$ reconstruction. Therefore, the PbO termination remains the most favorable.

The computed values for the Pb-O and Ti-O interlayer bond lengths are shown in Table V. The short and long Pb-O bonds are very similar due to the very small AFD rotation angles, and they are essentially equal at the surface where the rotation angle is zero within the accuracy of the calculation. The average bond length for each Pb atom is equal to the Pb-O bond length in the ideal perovskite structure (2.76 Å). The interlayer Ti-O bond lengths are very similar to those at the $c(2\times 2)$ and (1×1) PbO terminations (see Table III) indicating that they are independent of both termination and reconstruction.

C. Surface effect on the strength of the AFD instability

The energy gain associated with the lattice deformation is a measure of the strength of the instability, and can be used to compare the strength of the AFD instability at the PbO-surface with the one in the bulk.

The energy gain associated with the AFD deformation in a slab can be defined as the difference between the energy of the relaxed (1×1) non-polar slab, in which by symmetry there is no octahedron rotation, and the energy of the relaxed $c(2\times 2)$ non-polar slab. This energy difference can be divided into a *bulk* and a *surface* contribution as follows:

$$2E^{(1\times 1)\text{slab}} - E^{c(2\times 2)\text{slab}} = N\Delta E_{\text{AFD}}^{\text{bulk}} + 4\Delta E_{\text{AFD}}^{\text{surf}}. \quad (1)$$

The bulk contribution, $N\Delta E_{\text{AFD}}^{\text{bulk}}$, is the energy gain associated with the bulk-like rotation of the inner “non-surface” octahedra, with N being the number of such bulk-like octahedra in the $c(2\times 2)$ unit cell (N=6 for the 11 layer slab). The surface contribution, $4\Delta E_{\text{AFD}}^{\text{surf}}$, is the energy gain associated with the rotation of the surface octahedra. The factor of four arises because in the unit cell of a $c(2\times 2)$ slab there are four surface octahedra, two at each surface of the slab. Using Eq. 1, and the computed values for the three energies: $E^{(1\times 1)\text{slab}}$, $E^{c(2\times 2)\text{slab}}$, and

TABLE IV: Structural parameters for the TiO_2 -terminated (001) surface of paraelectric PbTiO_3 films. Change in the interlayer distance, Δd_{ij} , and layer rumpling, η_i , in percent of the lattice constant a_{bulk} . Rotation angle, θ_i , of the oxygen squares in the TiO_2 layers. Relaxation energy relative to the ideal (1×1) surface, ΔE_{relax} , in eV per (1×1) surface unit cell.

	this work		Meyer et al. ^a
	$c(2\times 2)$	(1×1)	(1×1)
Δd_{12}	-4.3	-4.3	-4.4
Δd_{23}	+3.4	+3.3	+3.1
Δd_{34}	-1.2	-1.3	-0.6
Δd_{45}	+0.6	+0.5	
η_1	-3.2	-3.2	-3.1
η_2	+4.3	+4.3	+4.1
η_3	-1.0	-0.9	-0.7
η_4	+0.9	+0.9	
η_5	0.0	0.0	
θ_1	-0.1°	0	0
θ_3	-2.1°	0	0
θ_5	2.8°	0	
(θ_{bulk})	(3.3°)		
ΔE_{relax}	-0.26	-0.26	

TABLE V: Pb-O and Ti-O interlayer bond length in Å computed for the TiO_2 termination of the $c(2\times 2)$ PbTiO_3 (001) surface. Average Pb-O bond lengths are also reported. We use the same notation as in Table III. The in-plane Pb-O bond lengths are 2.76 Å long.

Pb_i-O_j	short	long	average	Ti_i-O_j	
Pb_2-O_1	2.62	2.63	2.76	Ti_1-O_2	1.80
Pb_2-O_3	2.85	2.95		Ti_3-O_2	2.02
Pb_4-O_3	2.67	2.78	2.76	Ti_3-O_4	1.90
Pb_4-O_5	2.72	2.86		Ti_5-O_4	1.95

$\Delta E_{\text{AFD}}^{\text{bulk}}$, we find that the energy associated with the surface AFD distortion at the PbO-termination is $\Delta E_{\text{AFD}}^{\text{surf}} = 109$ meV per (1×1) surface unit cell.

By comparing this result with the AFD and FE well depths in the bulk (1.2 meV and 50 meV, respectively) we find that the energy gain associated with the surface AFD rotation is two orders of magnitude larger at the PbO-terminated surface than in the bulk, and about twice the bulk ferroelectric well depth.

V. IN-PLANE POLARIZED PbTiO_3 (001) FILMS

In this section we present our results for the $c(2\times 2)$ PbTiO_3 (001) film with spontaneous polarization paral-

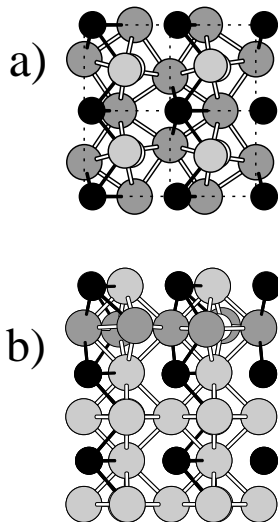


FIG. 4: Optimized atomic structure of the in-plane polarized $c(2 \times 2)$ (001) PbTiO_3 film with PbO surface termination. (a) Top view; only the first top two layers are shown. (b) Side view; only the top half of the 11-layer slab is shown. The oxygen atoms in the second layer are shown in a darker shade of gray. The in-plane Pb off-centering as well as the $c(2 \times 2)$ AFD O-rotation in the TiO_2 subsurface layer, are clearly visible. Pb-O bonds shorter than 2.6 Å are shown in black.

parallel to the surface, $\mathbf{P}=\text{P}(100)$. In particular we are interested in studying the interaction between AFD and in-plane FE distortions in proximity of the (001) surface. We consider only the PbO termination, which is the most energetically favorable and, as we have shown in the previous section, displays a strong surface AFD instability in absence of FE distortions.

The optimized atomic structure of the $c(2 \times 2)$ in-plane polarized film is shown in Fig. 4. Clearly visible are: (i) the in-plane Pb off-centering, present throughout the film and enhanced at the surface, and (ii) the large AFD TiO_4 rotation in the TiO_2 subsurface layer. Thus, contrary to the bulk where FE distortions suppress the AFD rotation, FE and AFD distortions coexist at the PbO surface.

We now consider these coupled distortions in more detail, using a symmetry analysis. The $c(2 \times 2)$ supercell can accommodate atomic distortions of the (1×1) ideal unit cell with wavevectors $\mathbf{q}=(000)$ and $\mathbf{q}=(110)\pi/a$ ($\bar{\Gamma}$ and \bar{M} point of the (1×1) surface BZ, respectively). Thus, the atomic displacements relative to the ideal perovskite structure can be decomposed into $\bar{\Gamma}$ - and \bar{M} -point irreducible representations of the reference (1×1) unit cell: $\delta_{\alpha,i} = \sum_{\nu} \delta_{\alpha,i}^{\nu}$ (where ν labels the irreducible representations, i the atoms in the $c(2 \times 2)$ unit cell, and $\alpha=x, y, z$). This decomposition allows us to separate the FE, AFE, and AFD contributions to the lattice distortion. We find that the in-plane atomic displacements can be decomposed into three irreps M_{3+} , M_{5-} , and Γ_{5-} (or E_u), which correspond to AFD, AFE, and FE distortions, respectively. The atomic displacement patterns

for the M_{3+} , M_{5-} , and Γ_{5-} irreducible representations are shown in Fig. 5(a-c).

To quantify, layer-by-layer, the strength of the AFD, AFE, and FE distortions we proceed as follows. The layer-by-layer strength of the AFD contribution is described by the TiO_4 rotation angle, θ , in each TiO_2 layer (see Fig. 5d). For the FE ($\nu=\Gamma_{5-}$) and AFE ($\nu=M_{5-}$) contributions we define the average polar distortion along the α -direction, p_{α}^{ν} , in each (1×1) unit cell of each atomic layer (see Fig. 5e-f); for TiO_2 layers

$$p_{\alpha}^{\nu} = \delta_{\alpha}^{\nu}(\text{Ti}) - \frac{[\delta_{\alpha}^{\nu}(\text{O}_I) + \delta_{\alpha}^{\nu}(\text{O}_{II})]}{2}, \quad (2)$$

and for PbO layers

$$p_{\alpha}^{\nu} = \frac{[\delta_{\alpha}^{\nu}(\text{Pb}_I) + \delta_{\alpha}^{\nu}(\text{Pb}_{II})]}{2} - \delta_{\alpha}^{\nu}(\text{O}), \quad (3)$$

where δ_{α}^{ν} are the atomic displacements in the $\alpha = x, y$ direction relative to the ideal (1×1) perovskite structure, for each irrep ν . For a film with spontaneous polarization along x , the average FE polar distortion is along x , p_x^{FE} , and has the same sign in each (1×1) unit cell, while the average AFE polar distortion is along y , p_y^{AFE} , and has opposite sign in each neighboring (1×1) unit cell.

The computed values for the parameters describing the strength of FE, AFE, and AFD distortions in each atomic layer are summarized in Table VI. The FE distortion is enhanced at the surface and rapidly resumes the bulk value in the inner layers. The average polar distortion in the first PbO layer is 1.7 times larger than the corresponding quantity in the bulk, and the enhancement is confined to the surface layer. The same behavior for the in-plane FE distortion was found at the (1×1) PbO-terminated surface,⁵ where AFD distortion is not allowed by symmetry. There, the average in-plane polar distortion in the first surface layer was found to be 1.5 times larger than the corresponding quantity in the bulk. It should be noted that in that calculation, the in-plane lattice parameters of the slab were taken as the bulk tetragonal c and a parameters, and the comparison is to the tetragonal bulk polarization. In our calculation, we fixed the in-plane lattice parameters to match a substrate of bulk cubic PbTiO_3 . The proper reference bulk limit in this case is the cubic lattice optimized allowing a spontaneous polarization along the (100) direction (i.e. allowing internal atomic displacements along (100)). The resulting ‘‘cubic polarized’’ structure (C-FE) is the bulk reference limit in Table VI.

The AFD oxygen-rotation is also enhanced at the surface, $\theta_2=10.8^\circ$, and rapidly vanishes in the deeper layers. Thus, the AFD distortion is confined to the surface octahedron layer, and is comparable to the one found in absence of FE distortions.

Finally, there is a small AFE distortion at the PbO surface layer that rapidly decreases in the inner layers where it is essentially zero.

TABLE VI: The average layer-by-layer ferroelectric, p_x^{FE} , and antiferroelectric, p_y^{AFE} , polar distortions per (1×1) unit cell, in percentage of the bulk lattice parameter ($a_b = 7.37 \text{ \AA}$), and the anti-ferrodistortive oxygen rotation, θ^{AFD} , in the TiO_2 layers. The average spontaneous polar distortion and the AFD angle computed for the bulk “polarized cubic” structure (C-FE) and the bulk “cubic AFD” structure (C-AFD) are given as a bulk reference.

layer	p_x^{FE}		p_y^{AFE}		θ^{AFD}
	TiO_2	PbO	TiO_2	PbO	
1		11.9		-2.4	
2	4.1		0.5		10.8°
3		6.3		0.4	
4	3.7		-0.06		-0.1°
5		7.1		-0.2	
6	3.9		0.08		0.9°
bulk (C-FE)	4.1	7.1			0°
bulk (C-AFD)	0.0	0.0			3.3°

The FE and AFD distortions have both the effect of shortening some of the Pb-O bonds. At the surface, the compounded effect of the coexisting large FE and AFD distortions results in even shorter Pb-O bonds, as short as 2.31 \AA (comparable to the shortest bondlength in PbO bulk).

VI. CONCLUSIONS

Non-polar cubic PbTiO_3 bulk has a weak AFD instability, involving rotations of oxygen octahedra, which is suppressed by the FE distortion. In this work we have studied the effect of surface proximity upon the AFD instability at the (001) surfaces of PbTiO_3 . In particular we studied the surface effect upon the instability’s strength and its competition with in-plane ferroelectricity.

In the absence of FE distortions we found that the impact of the surface upon the strength of the AFD instability is termination-dependent. At the PbO-termination the AFD deformation is strongly enhanced relative to the bulk; the top surface octahedra rotate by 11° about the surface normal. The enhanced AFD distortion is confined to the octahedron layer at the top of the surface. We estimated that the energy gain associated with the octahedron rotation is two orders of magnitude larger at

the surface than in the bulk. At the TiO_2 -termination, the AFD deformation is essentially suppressed; the top surface octahedra (which are truncated) rotate by an angle of 0.1° . For both terminations the surface effect upon the AFD distortion is confined to the first octahedron-layer at the surface, and below the surface octahedra the AFD rotation recovers the small bulk-like value, $\approx 3^\circ$, computed for non-polar cubic PbTiO_3 .

For polarized films (with in-plane FE distortion) we found that FE and AFD distortions coexist in the proximity of the PbO-terminated surface, leading to a structural phase not found in bulk. The FE distortion is enhanced at the surface layer as was previously found for the (1×1) films where the AFD distortions are not allowed by symmetry. Concurrently, the AFD distortion is enhanced at the surface as much as found in absence of FE distortions. Thus, AFD and in-plane FE distortions are both enhanced at the PbO surface and do not strongly interact. The enhanced AFD deformation does not suppress the FE distortion, nor is the AFD deformation suppressed by the FE distortion.

The surface effects are confined to the first perovskite unit cell at the surface (i.e. in the first three atomic layers), while bulk-like behavior is recovered below it.

In summary, we have shown that in PbTiO_3 the strength of the AFD instability, consisting of rotation of the oxygen octahedra, and its interaction with ferroelectricity are affected by the proximity to the surface. At the PbO termination this leads to a phase, not observed in the bulk, where enhanced AFD and FE distortions coexist. The enhancement of the AFD instability at the PbO termination is driven by the formation of shorter PbO bonds and is a consequence of the particular chemistry of Pb; no enhanced AFD distortion is found, for example, at the surface of BaTiO_3 . We suggest that the enhancement of the AFD instability at the PbO termination should be common among Pb based perovskite oxides.

ACKNOWLEDGMENTS

We thank D. Vanderbilt, G.B. Stephenson, C. Thompson, and D.D. Fong for discussions and Krzysztof Rapcewicz for a critical reading of the manuscript. This work was supported by Office of Naval Research through N00014-00-1-0261. The majority of computations were performed at the Department of Defense High Performance Computing Centers NAVO and ERDC.

* Electronic address: bungaro@physics.rutgers.edu

¹ W. Zhong and D. Vanderbilt, Phys. Rev. Lett. **74**, 2587 (1995).

² N. Sai and D. Vanderbilt, Phys. Rev. B **62**, 13942 (2000).

³ Ph. Ghosez, E. Cockayne, U.V. Waghmare, and K.M. Rabe, Phys. Rev. B **60**, 836 (1999).

⁴ J. Padilla and D. Vanderbilt, Phys. Rev. B **56**, 1625 (1997).

⁵ B. Meyer, J. Padilla, and D. Vanderbilt, Faraday Discuss. **114**, 395 (1999).

⁶ B. Meyer and D. Vanderbilt, Phys. Rev. B **63**, 205426 (2001).

⁷ A. Munkholm, S.K. Streiffer, M.V. Ramana Murty, J.A.

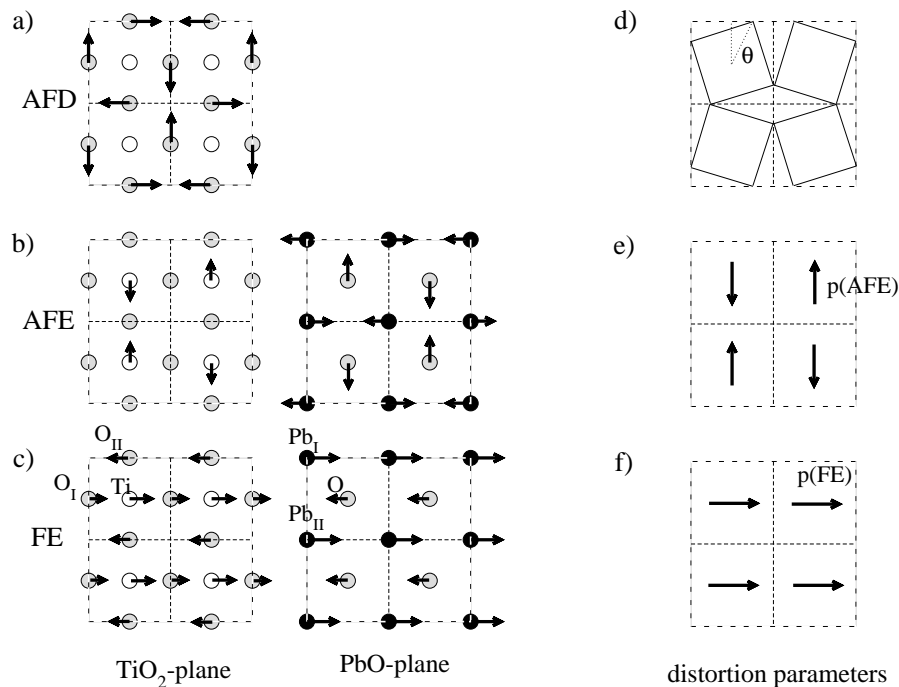


FIG. 5: (a), (b), and (c) atomic displacements, in the TiO_2 and PbO planes, for the AFD (M_{3+}), AFE (M_{5-}), and FE (Γ_{5-}) irreducible representations that contribute to the ground state structure of the in-plane polarized film. (d), (e), and (f) schematic representation of the layer-by-layer distortion parameters (see text) for AFD, AFE, and FE irreps, respectively. Dashed lines indicate the (1×1) unit cells.

Eastman, C. Thompson, O. Auciello, L. Thompson, J.F. Moore, and G.B. Stephenson, *Phys. Rev. Lett.* **88**, 16101 (2002).

⁸ S. Baroni, A. Dal Corso, S. de Gironcoli, and P. Giannozzi, <http://www.pwscf.org>.

⁹ D. M. Ceperley and B. J. Alder, *Phys. Rev. Lett.* **45**, 566 (1980); J. P. Perdew and A. Zunger, *Phys. Rev. B* **23**, 5048 (1981).

¹⁰ D. Vanderbilt, *Phys. Rev. B* **41**, R7892 (1990).

¹¹ H. J. Monkhorst and J. D. Pack, *Phys. Rev. B* **13**, 5188 (1976).

¹² The centrosymmetric $P2/m$ space group consists of: the identity (xyz), the inversion symmetry ($\bar{x}\bar{y}\bar{z}$), the 180° rotation C_{2z} ($\bar{x}\bar{y}z$), and the mirror symmetry M_z ($x\bar{y}\bar{z}$), relative to the center of the slab.

¹³ The Pm space group consists of two symmetry operations: the identity (xyz), and a mirror plane ($x\bar{y}\bar{z}$).

¹⁴ For the case of perpendicular polarization it is necessary to introduce a dipole layer in the vacuum region to cancel the artificial field arising when a slab with a net surface dipole

density is embedded in a periodic supercell (see Ref. 19). This dipole correction can be used, as shown in Ref. 6, to study the effect of external electric field on the equilibrium ground state structure of polar films with polarization perpendicular to the surface, and determine their ferroelectric properties.

¹⁵ A. García and D. Vanderbilt *Phys. Rev.* **B 54**, 3817 (1996).

¹⁶ This is our theoretical value. The experimental value for the shortest Pb-O bonds in tetragonal PbTiO_3 is 2.5\AA from Refs.[20,21].

¹⁷ R. E. Cohen, *Nature* **358**, 136 (1992).

¹⁸ H. J. Terpstra, R. A. de Groot, and C. Haas, *Phys. Rev. B* **52**, 11690 (1995).

¹⁹ L. Bengtsson, *Phys. Rev. B* **59**, 12301 (1999).

²⁰ G. Shirane, R. Pepinsky, and B.C. Frazer, *Acta Cryst.* **9**, 131 (1956).

²¹ W. Dmowski, M.K. Akbas, P.K. Davies, and T. Egami, *J. Phys. Chem. Solids* **61**, 229 (2000).